Carbon Dioxide Quantification in Human Breath Using Infrared Thermography

Vitor Furtado Paes[1,2], Jucélia Nascimento Rosa[1,2], Matheus Pereira Porto[1,2]

[1]Graduate Program in Mechanical Engineering (PPGMEC),
Universidade Federal de Minas Gerais, Brazil.

[2]Centro Multiusuário de Termografia Científica (CEMTEC),
Universidade Federal de Minas Gerais, Brazil

vitorpaes@ufmg.br, jucelianascimento@ufmg.br, matheusporto@ufmg.br

Abstract. *Carbon dioxide concentration in exhaled breath is a clinical metric for assessing respiratory and metabolic function. However, traditional capnography systems require physical contact, which can cause patient discomfort. This paper presents an exploratory investigation into the use of quantitative optical gas imaging as a non-invasive, remote sensing alternative for dynamically estimating CO_2 in human breath. A pilot study was conducted using a cooled mid-wave infrared thermographic camera and a narrow-bandpass filter. The results revealed peak CO_2 concentrations of approximately 50,000 ppm (5%) during nasal exhalation, consistent with standard physiological end-expiratory baseline ranges.*

1. Introduction

Carbon dioxide (CO_2) concentration in exhaled breath is a health metric for assessing respiratory function. CO_2 originates from blood via passive diffusion across the pulmonary alveolar membrane, and variations in this concentration can indicate pulmonary or metabolic diseases [Lou et al. 2019]. Under normal conditions, it reaches a peak end-expiratory concentration ($EtCO_2$) of 5% to 6% [Ghorbani and Schmidt 2017, Gerlach et al. 2019], which can increase by 60% to 110% during physical exertion [Lou et al. 2019].

The clinical application of exhaled CO_2 monitoring began in the 1950s for anesthesia management, though its widespread integration into medical practice only occurred in the early 1980s following the development of more compact devices [CK 2025]. Modern CO_2 monitoring devices are primarily categorized as either capnometers or capnographs, both types employ either infrared absorption or mass spectrometry to measure carbon dioxide [Dervieux et al. 2022]. While both instruments quantify gas concentrations, they differ significantly in their output displays. A capnometer provides a discrete numerical value for $EtCO_2$, whereas a capnograph delivers both a numerical reading and a continuous real-time waveform throughout the entire inspiratory-expiratory cycle.

Despite their widespread use, traditional capnography systems present inherent limitations in clinical practice. Devices require physical contact with the patient via endotracheal tubes, nasal cannulas, or facial masks, which can cause significant discomfort, particularly in pediatric patients. Furthermore, technical challenges persist in accurately capturing the rapid CO_2 signals of neonates, as these patients require exceptionally fast sensors and low suction flows for sidestream measurements [Schmalisch 2016].

In this context, this study presents an exploratory investigation into the use of quantitative optical gas imaging (OGI) to dynamically estimate CO_2 concentrations in exhaled breath. The passive optical gas imaging provides a non-invasive remote sensing alternative with the capability of spatially resolved measurements [Kang et al. 2022]. Specifically, this paper explores an approach for the quantitative estimation of CO_2 in human breath utilizing a cooled mid-wave infrared (MWIR) thermographic camera equipped with a specific narrow-bandpass CO_2 filter. By leveraging the camera's high thermal sensitivity and fast acquisition rates, the proposed method achieves both spatial and temporal resolution of the exhaled plume. This enables contactless gas quantification, ultimately offering a new perspective for continuous respiratory monitoring.

2. Methods

This section outlines the experimental and analytical approaches adopted to estimate CO_2 in exhaled breath over time. In this study, an InSb cooled thermal camera was used, equipped with a narrow-bandpass filter featuring a center wavelength of 4.265 μm and a half-width of 80 nm. The experiments were conducted in a controlled environment at the *Centro Multiusuário de Termografia Científica (CEMTEC)* at UFMG, Brazil. The methodology begins with the camera calibration procedure, described in Subsection 2.1, followed by a detailed description of the quantification method employed in Subsection 2.2.

2.1. Calibration

The FLIR x6801sc camera, equipped with the CO_2 filter, was calibrated using the SR-800N flat-plate blackbody radiator as a standard source of uniform radiance. The camera was positioned at a distance of 1 m from the blackbody, and 100 thermograms were captured for each temperature set point. For the purpose of this study, the calibration was performed over a temperature range of 80°C to 110°C in increments of 10°C. Simultaneously, environmental parameters, including ambient temperature, pressure, relative humidity, and atmospheric CO_2 concentration, were continuously monitored and recorded using a Testo 440 digital thermohygrometer.

A radiometric model was applied to calculate the total radiance reaching the camera detector for each calibration point. This model incorporates the radiance emitted by the blackbody radiator, the radiance from the surrounding environment reflected by the blackbody surface, and the atmospheric radiance emitted along the optical path. Equation 1 provides the mathematical formulation used to estimate the total radiation reaching the detector [Paes et al. 2025].

$$L_d = \int_{\lambda_1}^{\lambda_2} \tau_{lens,\lambda}\tau_{filter,\lambda}R_\lambda \left[L_\lambda(T_{bb})\varepsilon_{bb,\lambda}\tau_{atm,\lambda} + L_\lambda(T_{refl})\rho_{bb,\lambda}\tau_{atm,\lambda} + L_\lambda(T_{atm})\varepsilon_{atm,\lambda} \right] d\lambda, \tag{1}$$

where L, T, ε, ρ, and τ represent radiance, absolute temperature, emissivity, reflectivity, and transmissivity, respectively. The terms λ_1 and λ_2 define the operational wavelength range of the camera. The subscripts d, bb, refl, atm, and λ refer to the detector, blackbody, reflection, atmosphere, and spectral dependence, respectively.

The system's optical and detector characteristics, such as lens spectral transmissivity ($\tau_{lens,\lambda}$), filter spectral transmissivity ($\tau_{filter,\lambda}$), and detector spectral response (R_λ), are parameters provided by their respective manufacturers' datasheets. In contrast, the atmospheric spectral transmissivity ($\tau_{atm,\lambda}$) is obtained using the HITRAN Application Programming Interface (HAPI) via a line-by-line analysis, as it is a function of relative humidity, carbon dioxide concentration, atmospheric temperature, pathlength, wavelength interval, and spectral resolution [Gordon et al. 2022].

The radiative terms in Equation 1 are derived using Planck's Law, as expressed in Equation 2:

$$L_\lambda(T) = \frac{2hc_0^2}{\lambda^5 \left(e^{\frac{hc_0}{k_b \lambda T}} - 1 \right)}, \tag{2}$$

where L_λ is the spectral radiance, h is Planck's constant, c_0 is the speed of light in a vacuum, and k_b is Boltzmann's constant.

The camera calibration function, $L_d(C)$, establishes the relationship between the radiometric signal (L_d), calculated via Equation 1, and the raw digital signal (C). In this study, the relationship between the output digital signal and the incident radiation is well described by a linear function due to the narrow calibration range, expressed as:

$$L_d(C) = a_1 C + a_0, \tag{3}$$

where a_1 and a_0 are the fitting coefficients, determined by minimizing the sum of squared errors against the experimental data. This calibration equation provides the calibration coefficients that convert raw digital signal into radiance measurements.

2.2. CO_2 Quantification Procedure

Following the radiometric calibration of the infrared camera, the system was used to quantify carbon dioxide concentrations in human breath. This subsection details the methodology employed for this task, encompassing the data acquisition process, described in Subsubsection 2.2.1, and the subsequent data processing and analysis required to convert the raw digital counts into CO_2 column densities, detailed in Subsubsection 2.2.2.

2.2.1. Experimental Setup

To dynamically quantify the exhaled CO_2, a pilot study was conducted under monitored environmental conditions. A human subject was positioned directly in front of the blackbody radiator, which was initially set to a constant temperature of $110\,^{\circ}\mathrm{C}$ to provide a stable, high-radiance background. The subject was instructed to remain as static as possible to minimize motion artifacts during the image acquisition.

The infrared camera recorded sequences of thermograms capturing the gas plume under two distinct respiratory conditions: exhalation performed exclusively through the mouth, followed by exhalation through the nose. Simultaneously, a Testo 440 digital thermohygrometer recorded the baseline atmospheric carbon dioxide concentration, as well as ambient temperature, atmospheric pressure, and relative humidity.

A critical parameter required for the subsequent radiometric modeling is the temperature of the exhaled gas (T_{gas}). To estimate this value experimentally, a zero-contrast approach was employed prior to the main recordings. The subject breathed directly in front of the blackbody radiator while its temperature was systematically varied. The specific temperature setpoint at which no thermal contrast was observed between the exhaled gas plume and the background emitter's plate was recorded as the effective T_{gas}.

2.2.2. Radiometric Data Processing

During the post-processing phase, specific Regions of Interest (ROIs) were defined in the immediate vicinity of the subject's mouth and nose. The mean digital counts within these ROIs were extracted frame-by-frame to generate the raw temporal profiles of the exhaled plumes. Subsequently, the time-series digital counts extracted from the ROIs were converted into radiance using the previously established camera calibration function. Figure 1 shows the regions of interest positioned near the mouth and nose to capture the highest concentration of the exhaled plume.

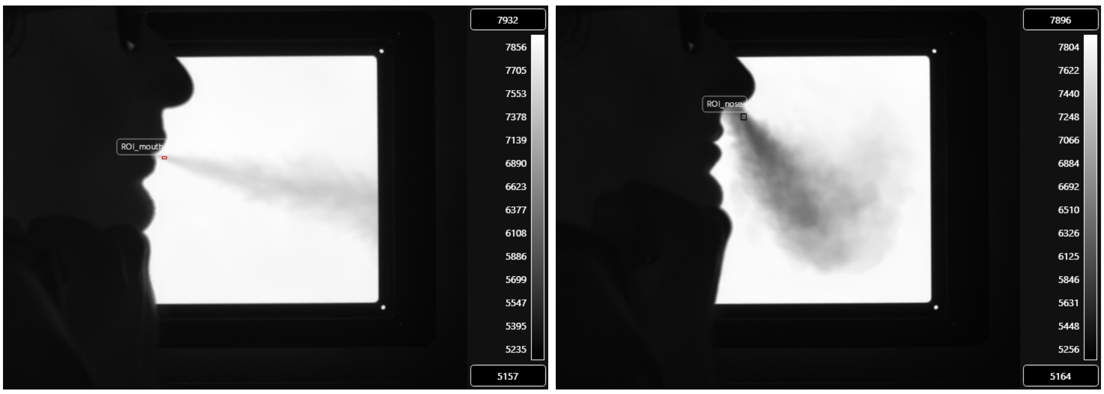

(a) (b)

Figure 1. Regions of interest positioned for capturing exhaled breath from (a) the mouth and (b) the nose.

To correlate the measured radiance with the gas concentration, a radiometric model was utilized. This model accounts for an additional atmospheric layer of CO_2 located between the camera and the blackbody source, which emits radiation due to its own temperature and further attenuates the radiation emitted by the background and the exhaled plume. The full radiometric model applied to this case study is defined as:

$$L_{d,\lambda} = \int_{\lambda_1}^{\lambda_2} \tau_{lens,\lambda}\tau_{filter,\lambda}R_\lambda \Big[L_\lambda(T_{bg})\varepsilon_{bg,\lambda}\tau_{gas,\lambda}\tau_{atm,\lambda} + L_\lambda(T_{refl})(1-\varepsilon_{bg,\lambda})\tau_{gas,\lambda}\tau_{atm,\lambda} + \cdots$$
$$\cdots + L_\lambda(T_{gas})\varepsilon_{gas,\lambda}\tau_{atm,\lambda} + L_\lambda(T_{atm})\varepsilon_{atm,\lambda} \Big] d\lambda, \quad (4)$$

where the subscripts bg, gas, and atm refer to the background, the exhaled CO_2 plume, and the atmospheric layer in front of the camera, respectively. Furthermore, $\tau_{atm,\lambda}$ represents the atmospheric transmissivity, derived from HITRAN, and $\tau_{gas,\lambda}$ is the transmissivity of the breathing gas layer, modeled according to the Beer-Lambert law as:

$$\tau_{gas,\lambda} = 1 - \varepsilon_{gas,\lambda} = e^{-\kappa_{\mathrm{CO}_2,\lambda} U_{\mathrm{CO}_2} 10^{-4}}, \quad (5)$$

where $\kappa_{\mathrm{CO}_2,\lambda}$ is the wavelength-dependent absorption coefficient of carbon dioxide in cm^{-1}, which was computed using the HITRAN database, and U_{CO_2} represents the CO_2 column path length, expressed in ppm · m. The 10^{-4} factor is required for dimensional consistency, converting the column path length from ppm · m to a dimensionless fraction multiplied by centimeters.

As indicated by Equations 3 and 5, determining the CO_2 column path length from the measured radiance constitutes an inverse radiative transfer problem. By iteratively varying the gas concentration ($\tau_{gas,\lambda}$) in Equation 5, a theoretical calibration curve was generated, establishing a direct relationship between the total incident radiance and the U_{CO_2}. Finally, the experimental radiance data were mapped onto this theoretical domain using linear interpolation, allowing for the dynamic, frame-by-frame estimation of the CO_2 column path length throughout the entire respiratory cycle.

Lastly, to extract the pure volumetric gas concentration in ppm from the calculated CO_2 column path length, the geometric depth of the plume must be considered. The absolute CO_2 concentration can be calculated by dividing the column path length by the optical depth, which is approximated as the average diameter of the exhalation source.

3. Results and Discussions

3.1. Calibration

Table 1 presents the experimental parameters, the digital counts obtained during the calibration procedure, and the total radiance reaching the detector calculated using the radiometric model. Figure 2 illustrates the resulting calibration curve, which demonstrates that a linear fit between the raw digital counts and the theoretical radiance is valid across the evaluated temperature range. The linear fit obtained is given by the equation $L = 0.00012 \times C - 0.569$.

Table 1. Experimental conditions for the calibration of the cooled infrared camera.

Set point (°C)	T_{atm} (°C)	UR (%)	CO_2 (ppm)	P_{atm} (Pa)	Signal -	Standard Deviation	Radiance (W/(sr m^2))	Standard Deviation (W/(sr m^2))
80	21.5	47.7	602	92110	6347	0.86	0.20	0.000104
90	21.5	47.4	602	92100	6790	1.17	0.25	0.000142
100	21.5	46.6	591	92110	7304	0.94	0.31	0.000114
110	21.3	44.6	602	92120	7895	1.59	0.39	0.000193

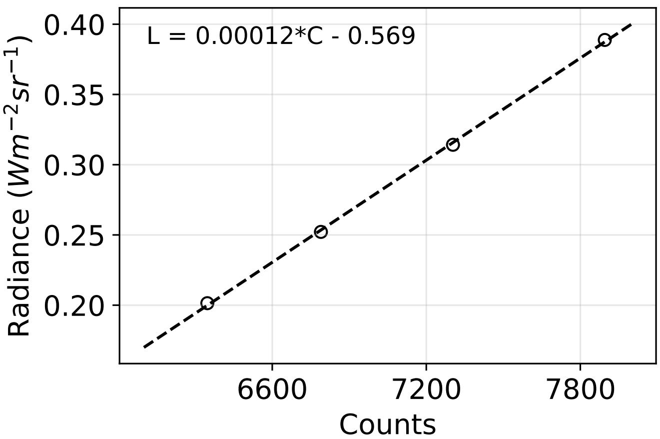

Figure 2. Calibration curve for radiance measurements. Calibration coefficients are displayed in the graph.

3.2. CO_2 Quantification

Figure 3 compares the estimated CO_2 column path length over time for both oral and nasal breathing. A substantial difference in signal magnitude is observed between the two respiratory pathways. While mouth breathing produced a column path length that stabilized around 240 ppm·m, nose breathing reached significantly higher values, ranging between 2,500 and 3,000 ppm·m.

Furthermore, Figure 4 illustrates the estimation of volumetric CO_2 concentration over time. During mouth breathing, the estimated concentrations reached approximately 25,000 ppm. In contrast, during nasal breathing, the system recorded peak concentrations around 50,000 to 60,000 ppm. A concentration of 50,000 ppm is equivalent to 5% CO_2 by volume, which aligns with the normal physiological end-expiratory carbon dioxide $EtCO_2$ baseline of 5% to 6% reported in the literature [Ghorbani and Schmidt 2017, Gerlach et al. 2019]. The agreement between the experimental OGI measurements and the expected physiological values is indicative of the method's potential.

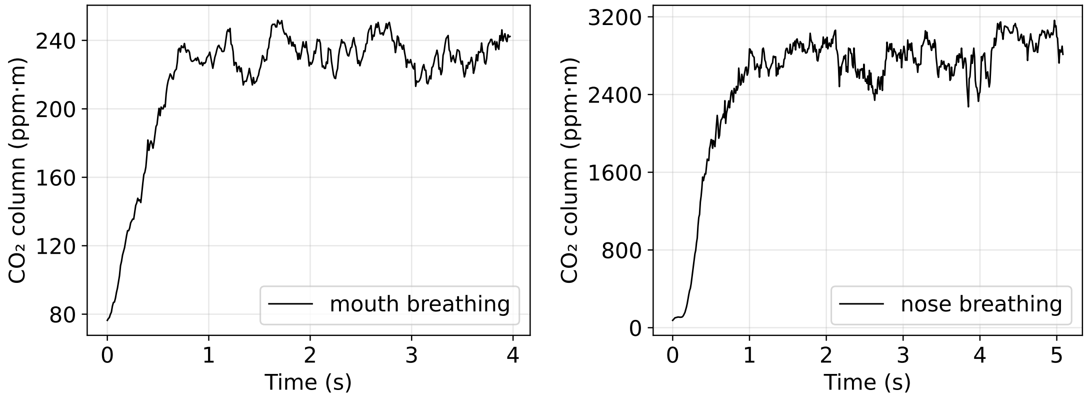

(a) **(b)**

Figure 3. Estimated CO_2 column over time, comparing exhaled breath from (a) the mouth and (b) the nose.

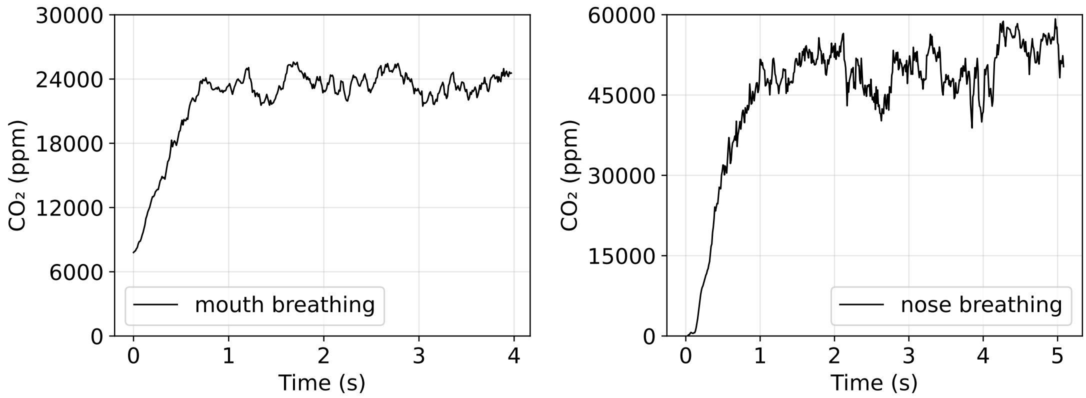

(a) **(b)**

Figure 4. Estimated CO_2 ppm over time, comparing exhaled breath from (a) the mouth and (b) the nose.

4. Conclusions

This exploratory pilot study demonstrated a non-invasive approach for the quantitative estimation of CO_2 in human breath using mid-wave infrared thermography. By implementing a rigorous radiometric calibration and a radiative transfer model, it was possible to dynamically quantify CO_2 concentrations without physical contact with the subject.

The results obtained show that peak concentrations during nasal exhalation reached approximately 50,000 ppm (5%), which is in high agreement with the physiological baseline of 5% to 6% expected for healthy individuals. This agreement between the experimental OGI measurements and the expected physiological values is indicative of the method's potential.

As an exploratory investigation, this work opens several avenues for future research. A critical next step is the analysis of measurement uncertainty to facilitate comparisons between different methodologies and to ensure metrological rigor. Furthermore, these results should be validated using measurements obtained with traditional techniques, such as chromatography or capnography, to better understand the limitations and detection limits of the proposed methodology. Finally, analyzing the temporal fluctuations and the shape of the CO_2 waveform throughout the entire respiratory cycle could provide valuable diagnostic insights into various pulmonary and metabolic diseases.

5. Acknowledgements

The authors acknowledge the Centro Multiusuário de Termografia Científica (CEMTEC) for providing the necessary infrastructure for this research. This study was financed in part by Fundação de Amparo à Pesquisa do Estado de Minas Gerais (FAPEMIG), Financiadora de Estudos e Projetos (FINEP), Coordenação de Aperfeiçoamento de Pessoal de Nível Superior (CAPES), Conselho Nacional de Desenvolvimento Científico e Tecnológico (CNPq), and by the Pró-Reitoria de Pesquisa da Universidade Federal de Minas Gerais (PRPq).

References

CK, S. S. (2025). To assess the effect of planned teaching programme on knowledge regarding the end-tidal carbon dioxide monitoring among the student nurses from a selected college in mumbai. *A and V Pub International Journal of Nursing and Medical Research*, 4(1):20–24.

Dervieux, E., Théron, M., and Uhring, W. (2022). Carbon Dioxide Sensing—Biomedical Applications to Human Subjects. *Sensors*, 22(1).

Gerlach, G., Guth, U., and Oelßner, W. (2019). *Carbon dioxide sensing: fundamentals, principles, and applications*. John Wiley & Sons.

Ghorbani, R. and Schmidt, F. M. (2017). Real-time breath gas analysis of CO and CO2 using an EC-QCL. *Applied Physics B*, 123.

Gordon, I. E., Rothman, L. S., Hargreaves, e. R., Hashemi, R., Karlovets, E. V., Skinner, F., Conway, E. K., Hill, C., Kochanov, R. V., Tan, Y., et al. (2022). The HITRAN2020 molecular spectroscopic database. *Journal of quantitative spectroscopy and radiative transfer*, 277:107949.

Kang, R., Liatsis, P., and Kyritsis, D. (2022). Emission quantification via passive infrared optical gas imaging: A review. *Energies*.

Lou, C., Jing, C., Wang, X., Chen, Y., Zhang, J., Hou, K., Yao, J., and Liu, X. (2019). Near-infrared tunable diode laser absorption spectroscopy-based determination of carbon dioxide in human exhaled breath. *Biomedical optics express*, 10 11:5486–5496.

Paes, V. F., Rosa, J. N., Costa, P. B., Ferreira, R. A. M., and Porto, M. P. (2025). Calibration of a cooled MWIR camera with a narrow-band filter for quantitative thermography. *Quantitative InfraRed Thermography Journal*, 0(0):1–20.

Schmalisch, G. (2016). Current methodological and technical limitations of time and volumetric capnography in newborns. *BioMedical Engineering OnLine*, 15.